APEM journal

Advances in Production Engineering & Management
Volume 21 | Number 1 | March 2026 | pp 57–74
https://doi.org/10.14743/apem2026.1.561

ISSN 1854-6250
Journal home: apem-journal.org
Original scientific paper

A data-to-decision framework for selecting turning conditions of C3604 brass

Le, V.-P.[a], **Nguyen, V.-H.**[a,*]

[a]Faculty of Mechanical Engineering and Mechatronics, Phenikaa University, Hanoi, Vietnam

ABSTRACT

This study presents a data-to-decision workflow that combines surrogate modeling, multi-objective optimization, and decision-making in a single procedure. Four surrogate models, including Kolmogorov–Arnold Networks (KAN), CatBoost (CAT), Gradient Boosting Regressor (GBR), and LightGBM (LGB), were trained under a unified preprocessing and Bayesian tuning scheme and evaluated on held-out data. The retained models were then embedded in NSGA-III to generate the Pareto front for the trade-off between surface roughness (*Ra*) and material removal rate (*MRR*). To move from the Pareto set to a single operating condition, the candidate solutions were further assessed using multiple MCDA methods under different objective weighting schemes, and the resulting rankings were combined through rank aggregation (Borda, Copeland, Kemeny–Young, Robust Rank Aggregation). A turning case study on C3604 free-cutting brass, using cutting speed, feed, depth of cut, nose radius, and coolant condition as inputs, showed that the final recommendation remained stable across different weighting and ranking settings. Experimental verification at selected Pareto points agreed well with the predicted values, with relative errors of about 5 % for both *Ra* and *MRR*. The results show that the proposed workflow provides a practical and consistent route from limited machining data to a final operating decision.

ARTICLE INFO

Keywords:
C3604 brass;
Data-to-decision;
Surrogate modeling;
Kolmogorov–Arnold network (KAN);
NSGA-III;
MCDA;
Machining optimization;
Multi-objective optimization

**Corresponding author:*
hai.nguyenvan1@phenikaa-uni.edu.vn (Nguyen, V.-H.)

Article history:
Received 5 April 2026
Revised 16 April 2026
Accepted 19 April 2026

1. Introduction

Optimizing machining parameters remains a core need in modern manufacturing because practitioners must simultaneously satisfy diverse performance targets—surface integrity, tool consumption, throughput, mechanical loads (forces and power), and increasingly energy-related indicators—under real shop-floor constraints involving machine capability, tool geometry, coolant strategy, and safety. The problem is inherently multi-objective and constraint-laden, so it benefits from decision processes that make trade-offs explicit and reproducible, rather than relying on ad hoc tuning. Recent studies in the field underscore both the energy and efficiency imperative and the practicality of multi-objective modeling and optimization in machining applications, reinforcing the need for auditable, data-driven parameter selection [1-3].

Machining datasets are often small, heterogeneous, and strongly affected by setup-dependent variation, which makes reliable parameter selection difficult even before the optimization stage is considered. In machining experiments, continuous cutting variables such as cutting speed, feed,

and depth of cut are commonly mixed with categorical factors such as coolant mode, insert geometry, and tool condition, while the measured outputs may also contain interaction effects, process noise, and metrology scatter [4]. Under these conditions, a single-stage analysis is usually not sufficient. A practically useful framework should first establish predictive surrogates that can generalize beyond the limited experimental runs, because overfitted models provide little value for downstream optimization or engineering decision-making [5].

Recent machining studies increasingly move toward an integrated route in which validated surrogate models are used to approximate process responses, evolutionary search is then employed to construct the trade-off surface among conflicting objectives, and a decision layer is finally introduced to identify an implementable operating point from the Pareto set [2, 6]. This shift is important because direct trial-and-error selection is inefficient in multi-factor machining problems, whereas optimization-only studies often stop at reporting Pareto fronts without resolving the final engineering choice in a transparent way [7].

When only a limited number of experiments are available, the predictive stage becomes one of the most critical parts of the workflow. Machining data often combine nonlinear process behavior with a mixture of continuous and categorical inputs, so different surrogate models may respond quite differently to the same dataset. In this setting, tree-based ensembles can be effective for structured tabular data, whereas neural or spline-based models may better capture smoother but coupled response patterns. Even so, no model should be assumed to be the best in advance for every machining response, and model selection needs to be based on actual predictive performance rather than preference or convention [8, 9]. This issue becomes even more important in multi-objective optimization, because the Pareto front is only as reliable as the surrogates used to construct it. If the retained models are unstable or locally biased, the optimization stage may still produce solutions that appear attractive numerically but are less trustworthy from a physical or machining perspective [10]. The same caution applies to the final decision stage. Obtaining a well-spread Pareto set does not automatically resolve which setting should be implemented, since the preferred solution may still change with the weighting scheme and ranking rule adopted. For that reason, transparent multi-criteria procedures and objective weighting methods are needed not only to compare alternatives, but also to make the final recommendation more stable and technically defensible [11, 12].

Recent studies have also demonstrated the practical value of combining modelling, optimization, and confirmation experiments in turning applications. For instance, recent work on dry turning of Inconel 625 [13] and Inconel 825 [14] reported effective optimization of quality-related and productivity-related responses under experimentally validated conditions. However, the transition from the optimized solution set to a final and methodologically robust engineering recommendation is still less explicitly addressed in many such studies.

Most machining studies do not carry the whole process through from prediction to optimization and then to final decision-making. Many papers stop after reporting model accuracy, while others present a Pareto front but leave the final choice to a single ranking method or a fixed set of weights. In such cases, it is difficult to know whether the recommended setting is genuinely robust or simply favored by one particular decision rule [2, 5]. This issue is more critical when the dataset is small, because any instability in the predictive model can carry over into the optimization stage and finally affect the selected solution. Another limitation is that convergence of the optimization algorithm and experimental confirmation of the chosen setting are not always reported together. Without both, the final recommendation may appear reasonable in computation, yet remain insufficiently supported from a machining point of view [15]. For this reason, a more complete data-to-decision workflow is still needed, one that links surrogate modeling, Pareto search, and the final selection step in a transparent and technically traceable way.

This study aims to establish a practical data-to-decision workflow for machining applications with limited experimental data. Rather than focusing on a single modeling or optimization technique, the work integrates surrogate modeling, multi-objective optimization, and MCDA into a consistent and traceable procedure. The objective is to ensure that the final recommended setting is not only accurate in prediction, but also stable under different decision assumptions.

The proposed framework is then examined through a turning case study on C3604 free-cutting brass, where *Ra* and *MRR* are considered as the primary objectives. This combination allows the study to evaluate both the predictive capability of the models and the robustness of the final decision in a realistic machining context.

This study develops an integrated data-to-decision workflow for machining parameter selection under limited data conditions. The proposed approach links surrogate modeling, multi-objective optimization, and multi-criteria decision-making within a single procedure, with particular attention to how the final solution is affected by model behavior and decision assumptions. Instead of relying on one surrogate model or a fixed ranking rule, the framework emphasizes consistency across the predictive, optimization, and selection stages, so that the recommended setting remains stable when different weighting or ranking strategies are considered. The workflow is then examined through a turning case study on C3604 brass, where the trade-off between *Ra* and *MRR* is used to evaluate both predictive performance and decision robustness.

2. Data to decision framework

The proposed framework provides a structured route for converting machining data into an implementable parameter recommendation. As illustrated in Fig. 1, the workflow consists of six linked stages, from data preparation to experimental confirmation of the selected solution. The purpose is not only to obtain accurate predictions, but also to ensure that the final operating point remains technically reasonable and robust at the decision stage.

2.1 Stage 1: Data acquisition and preprocessing

The first stage establishes the dataset used for model development. In machining applications, the data typically include controllable cutting parameters and measured performance responses, with both numerical and categorical variables appearing in the same dataset [1, 14]. In the present study, the dataset is formed from the designed turning experiments, using cutting speed, feed, depth of cut, nose radius, and coolant condition as inputs, and surface roughness and material removal rate as the main outputs. Before modeling, categorical variables are encoded, continuous variables are checked for consistency, and the data are split into training and test subsets. For the productivity response, *MRR* is calculated from turning kinematics, while Ra is obtained from post-process measurement [2].

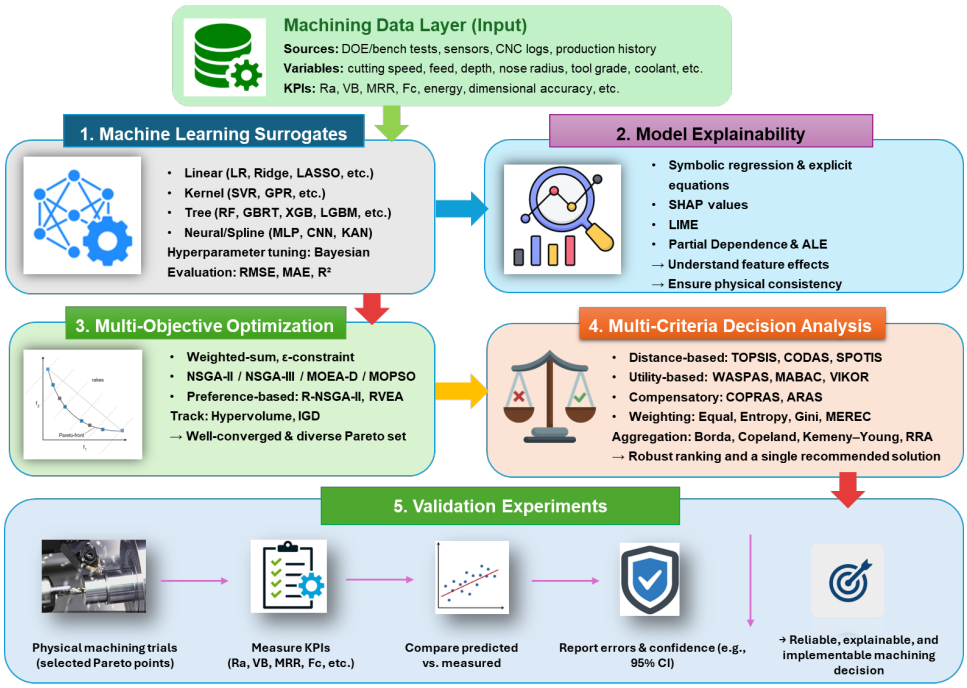

Fig 1 Generalized data-to-decision workflow for machining optimization

2.2 Stage 2: Machine-learning surrogate modeling

The second stage uses surrogate models to describe the relationship between machining inputs and outputs. This step is particularly important when the available dataset is limited, because the optimization stage requires fast and repeatable evaluation over the feasible design space [17]. Different model families may behave differently on the same machining dataset, especially when nonlinear effects and mixed input types are present [18]. Therefore, several candidate models are compared under the same preprocessing and tuning procedure, and their performance is evaluated using RMSE, MAE, and R^2. The best-performing surrogates are then retained for downstream optimization.

2.3 Stage 3: Model explainability

The third stage examines whether the retained models behave in a physically meaningful way. Explainability tools are used to identify the dominant input variables and to clarify how they influence the predicted responses [19]. For interpretable model forms such as KAN, the learned relationships can also be examined in a more explicit form [20]. This stage helps connect predictive performance with machining knowledge and reduces the risk of relying on numerically accurate but physically doubtful trends.

2.4 Stage 4: Multi-objective optimization

Once the surrogate models have been retained, they are used in a multi-objective optimization step to generate non-dominated machining conditions. In this study, the optimization seeks a balance between surface quality and productivity, represented by *Ra* and *MRR*. NSGA-III is employed to approximate the Pareto front, while convergence and spread are checked before the candidate solutions are passed to the decision stage [21].

2.5 Stage 5: Multi-criteria decision analysis

Because the Pareto front usually contains several feasible alternatives, a separate decision stage is needed to identify a single implementable setting. MCDA methods are therefore used to rank the Pareto candidates under defined weighting schemes [20-21]. Since the final ranking may vary with the weighting and scoring method, objective weighting and rank aggregation are included to reduce dependence on a single method and improve the robustness of the final recommendation [5].

2.6 Stage 6: Experimental validation

The final stage verifies the selected solutions experimentally. Representative Pareto points are retested under the same machining conditions, and the measured responses are compared with the predicted values using absolute and relative error [24]. This step is necessary to confirm that the selected operating point is not only favorable in computation, but also reliable in actual machining practice.

Overall, the framework links data preparation, surrogate modeling, explainability, optimization, decision analysis, and experimental confirmation in a single workflow. In this way, limited experimental data can be translated into a final machining recommendation that is both technically interpretable and practically verifiable.

3. A turning case study

To verify the practical applicability of the proposed data-to-decision framework, a turning case study was conducted on C3604 free-cutting brass. The study considers the main controllable parameters, including V_c, f, a_p, R_E, and CL, with the aim of balancing *Ra* and *MRR*. The following subsections describe the experimental setup and the implementation of the proposed workflow.

3.1 Experimental setup

Turning experiments were performed on a UGINT L2100 CNC lathe (11 kW spindle, automatic feed control). The work material was C3604 free-cutting brass, supplied as round bars of uniform hardness and diameter; cylindrical blanks (30 mm diameter, 100 mm length) were prepared. A

DCGT11304/08 AK carbide insert for non-ferrous alloys was mounted on a standard toolholder with controlled overhang and alignment.

A D-optimal (coordinate-exchange) design targeting a two-factor-interaction (2FI) model was generated with 40 randomized runs and no blocks. Five factors were studied, including V_c, f, a_p, and two categorical R_E and CL conditions. The discrete levels actually tested are listed in Table 1. Randomization was used to minimize temporal drift and nuisance effects.

Cutting parameters followed a designed matrix of V_c, f, a_p, R_E, and CL. Ra was measured after each run using a portable stylus profilometer (0.8 mm cutoff, 5 mm sampling length); the mean of three traces was recorded.

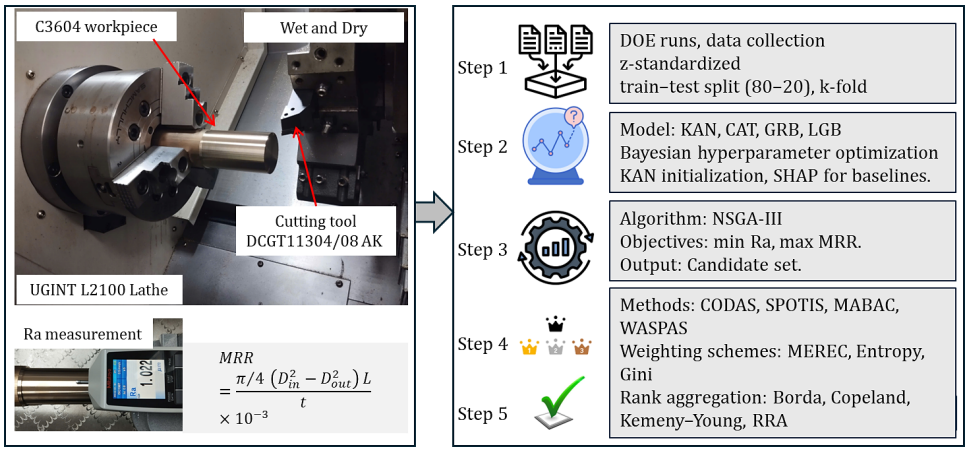

Fig 2 Integrated experimental setup and data-to-decision workflow for turning of C3604 brass

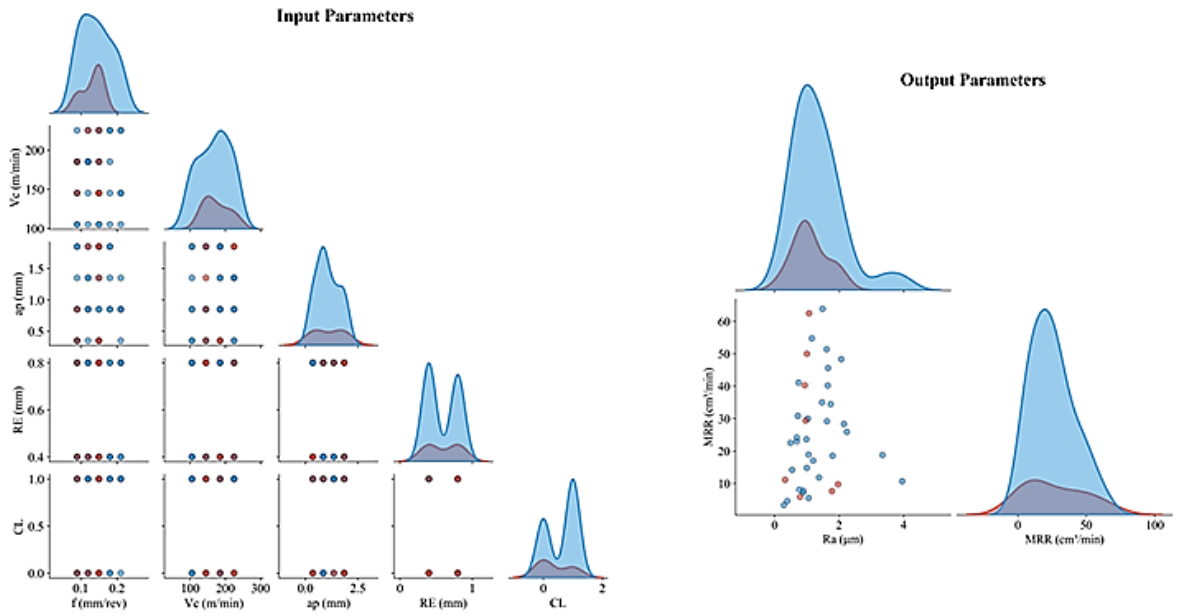

Fig. 3 Pairplot illustrating the distribution and overlap of train and test datasets for both input and output parameters in the C3604 turning experiment

Table 1 Experimental turning conditions

Parameter	Unit	Levels
Cutting speed (V_c)	m/min	105, 145, 185, 225
Feed (f)	mm/rev	0.09, 0.12, 0.15, 0.18, 0.21
Depth of cut (a_p)	mm	0.35, 0.85, 1.35, 1.85
Tool grade	–	Korloy DCGT11304/08
Coolant (CL)	–	“0” = Dry, “1” = Flood (emulsion 6-8 %),
Tool nose radius (R_E)	mm	“0” = 0.4 mm, “1” = 0.8 mm
Machine tool	–	UGINT L2100 CNC lathe

The material removal rate was computed from turning kinematics:

$$MRR = \frac{\pi/4\left(D_{in}^2 - D_{out}^2\right)L}{t} \times 10^{-3} \quad (1)$$

where D_{in} and D_{out} are the initial and final diameters (mm), L is the machined length (mm), and t is the machining time (min). Fig. 2 illustrates the overall setup, showing the brass workpiece, cutting tool configuration, and surface-roughness measurement arrangement. Meanwhile, Fig. 3 summarizes the input factors and output responses considered in the turning process.

3.2 Implementation of the data-to-decision workflow

Surrogate modeling

To model the mapping from machining inputs to performance responses, four surrogate models were considered, including KAN, CAT, GBR, and LGB.

KAN is based on the Kolmogorov–Arnold representation theorem, which states that a multivariate function can be represented as a superposition of univariate functions. Accordingly, a target function $f(x_1, \ldots, x_n)$ can be expressed as:

$$f(x_1, \ldots, x_n) = \sum_{q=1}^{2n+1} \Phi_q \left(\sum_{p=1}^{n} \phi_{q,p}\left(x_p\right) \right) \quad (2)$$

where $\phi_{q,p}(\cdot)$ and $\Phi_q(\cdot)$ are univariate functions.

In KAN, these functions are implemented as learnable spline-based mappings, replacing fixed activation functions used in conventional neural networks. This formulation allows the model to approximate complex nonlinear relationships while retaining a degree of interpretability, as the contribution of each input variable can be examined through the learned univariate functions.

In contrast, CAT, GBR, and LGB belong to the family of tree-based ensemble models, which are widely used for tabular datasets. These methods approximate the target function by combining multiple regression trees:

$$\hat{y}(x) = \sum_{k=1}^{K} f_k\left(x\right), f_k \in \mathcal{T} \quad (3)$$

where each f_k represents a decision tree. In boosting-based methods such as GBR and LGB, trees are added sequentially to minimize a loss function:

$$\hat{y}^{(t)}(x) = \hat{y}^{(t-1)}(x) + \eta f_t(x)$$

where η is the learning rate. LGB improves computational efficiency through histogram-based splitting, while CAT enhances performance on categorical variables using ordered boosting and encoding strategies.

Given the machining dataset

$$\mathcal{D} = \{(x_i, y_i)\}_{i=1}^{N} \quad (4)$$

with $x_i = \left[V_c, f, a_p, R_E, CL\right]$ and y_i represents the response Ra or MRR, the surrogate model approximates:

$$\hat{y} = \mathcal{F}(x; \theta) + \varepsilon \quad (5)$$

where $\mathcal{F}(x; \theta)$ is the regression model KAN, CAT, GBR, and LGB, θ are learnable parameters, and ε denotes model residuals.

Model parameters are estimated by minimizing the mean-squared error:

$$\min_{\theta} \mathcal{L}(\theta) = \frac{1}{N}\sum_{i=1}^{N}\left(y_i - \mathcal{F}(x_i; \theta)\right)^2 \quad (6)$$

For model development, the dataset was split into training and test subsets (80/20). A 5-fold cross-validation procedure was applied only within the training set for hyperparameter tuning, while the held-out test set was used for final model evaluation.

Hyperparameter optimization was performed using Bayesian optimization with a Gaussian Process surrogate $g(\lambda)$ to minimize the validation loss [25]:

$$\lambda^* = arg\min_{\lambda \in \Lambda} E[\mathcal{L}_{val}(\lambda)] \tag{7}$$

where λ denotes the hyperparameter vector. The next query point is selected by maximizing the Expected Improvement (EI), defined as follows [26]:

$$\mathrm{EI}(\lambda) = \big(\mu_{min} - \mu(\lambda)\big)\Phi(Z) + \sigma(\lambda)\phi(Z), \quad Z = \frac{\mu_{min} - \mu(\lambda)}{\sigma(\lambda)} \tag{8}$$

The model with the lowest cross-validated RMSE and the highest R^2 is retained for multi-objective optimization.

Bi-objective optimization

After the surrogate models for *Ra* and *MRR* were established, they were used in the optimization stage to search for machining conditions that balance surface quality and productivity. In this study, the problem involves two conflicting objectives:

$$\min_x f_1(x) = Ra(x), \qquad \max_x f_2(x) = MRR(x) \tag{9}$$

subject to operational bounds:

$$V_c \in \left(V_c^{min}, V_c^{max}\right), f \in \left(f^{min}, f^{max}\right) a_p \in \left(a_p^{min}, a_p^{max}\right), R_E \in (0,\ 1), CL \in (0{,}1).$$

A solution x is considered Pareto-optimal if there is no other feasible solution x' that gives a lower *Ra* and a higher *MRR* at the same time, with at least one of the two being strictly better. Accordingly, the Pareto-optimal set is defined as

$$P^* = \{x \in \Omega | \nexists x' \in \Omega : Ra(x') \le Ra(x), \forall j,\ MRR(x') \le MRR(x)\} \tag{10}$$

To obtain this set, NSGA-III was employed as the search algorithm. In the present study, NSGA-III works directly with the retained surrogate models instead of repeated physical trials, which makes it possible to examine a large number of candidate settings within the allowable parameter ranges. The resulting Pareto front represents the trade-off between finish and productivity, and its convergence behavior was monitored using hypervolume and IGD [21].

MCDA-based ranking

The Pareto solutions obtained from NSGA-III represent different trade-offs between *Ra* and *MRR*. Since only one operating condition is required in practice, these solutions were further ranked using MCDA.

Each Pareto solution was treated as an alternative, with *Ra* and *MRR* as the decision criteria. Because lower *Ra* is preferred while higher *MRR* is desirable, they were treated as cost-type and benefit-type criteria, respectively. The criteria were normalized to [0, 1] using for benefit-type:

$$f'_{\mathrm{ij}} = \frac{f_{\mathrm{ij}} - f_j^{\min}}{f_j^{\max} - f_j^{\min}} \tag{11}$$

and for cost-type criteria:

$$f'_{ij} = \frac{f^{max}j - fij}{f_j^{max} - f_j^{min}} \tag{12}$$

Values are $v_{ij} = w_j, f'_{ij}$, where w_j are objective weights.

To improve robustness, multiple MCDA methods (CODAS, SPOTIS, MABAC, and WASPAS) were combined with different objective weighting schemes (Entropy, Gini, and MEREC), and the final ranking was obtained from their aggregated results.

Objective weighting

Because the final ranking may depend on how much importance is assigned to *Ra* and *MRR*, three objective weighting schemes were considered in this study, namely Entropy, Gini, and MEREC. These methods were used to reduce reliance on a single weighting rule and to examine the stability of the final decision under different weighting perspectives.

For Entropy weighting [5], the normalized contribution of alternative i to criterion j is first defined as $p_{ij} = f'_{ij} / \sum_{i=1}^{n} f'_{ij}$. The entropy value is then calculated using with $k = 1/\ln\, n$ as the normalization coefficient:

$$H_j = -k \sum_{i=1}^{n} p_{ij} \ln p_{ij}\,, \qquad w_j = \frac{1 - H_j}{\sum_{k=1}^{m}(1 - H_k)} \tag{13}$$

For Gini weighting [27], the normalized values are sorted in ascending order, and the degree of dispersion for each criterion is measured by:

$$G_j = 1 - 2 \sum_{i=1}^{n} \frac{i}{n} p_{(i)j}, \qquad w_j = \frac{G_j}{\sum_{k=1}^{m} G_k} \tag{14}$$

For MEREC weighting [12], the average normalized value of criterion j is first written as $\overline{f'}_j = \frac{1}{N}\sum_{i=1}^{n} f'_{ij}$, and the corresponding weight is obtained from the deviation of each alternative from this average:

$$w_j = \frac{\sum_{i=1}^{n} \left| f'_{ij} - \overline{f'}_j \right|}{\sum_{k=1}^{m} \sum_{i=1}^{n} \left| f'_{ik} - \overline{f'}_k \right|} \tag{15}$$

These weighting schemes were applied separately before the MCDA scoring stage, so that the subsequent ranking could be examined under different objective-weighting conditions.

MCDA scoring

After determining the objective weights, each Pareto solution is evaluated using several MCDA methods to obtain comparable scores and rankings. In this study, four methods—CODAS, SPOTIS, MABAC, and WASPAS—are applied under the same normalized decision matrix.

For CODAS [28], the negative-ideal solution $f_j^* = \max_i f'_{ij}$ is used to compute Euclidean and taxicab distances, and the relative assessment score is formed as:

$$S_i = -\sqrt{\sum_{j=1}^{m} w_j \left(f'_{ij} - f_j^* \right)^2} + \tau \sum_{j=1}^{m} \left| f'_{ij} - f_j^* \right| \tag{16}$$

For SPOTIS [29], the distance of each alternative to the ideal point is calculated as:

$$D_i = \sqrt{\sum_{j=1}^{m} w_j \left(f'_{ij} - f_j^* \right)^2}, \qquad S_i = 1 - \frac{D_i - D_{min}}{D_{max} - D_{min}} \tag{17}$$

For MABAC [23], the deviation of each alternative from the border approximation area is evaluated, and the final score is obtained as:

$$S_i = -\sqrt{\sum_{j=1}^{m} w_j \left(f'_{ij} - f_j^* \right)^2} + \tau \sum_{j=1}^{m} \left| f'_{ij} - f_j^* \right| \tag{18}$$

and the final score is

$$S_i = \sum_{j=1}^{m} w_j \,, Q_{ij} \tag{19}$$

For WASPAS [22], the score combines additive and multiplicative aggregation:

$$S_i = \frac{1}{2}\sum_{j=1}^{m} w_j \frac{f'_{ij}}{f_j^*} + \frac{1}{2}\prod_{j=1}^{m} \left(\frac{f'_{ij}}{f_j^*} \right)^{w_j} \tag{20}$$

Each method produces a ranking of the Pareto solutions. These rankings are then used in the subsequent aggregation step to obtain a consensus decision.

Rank aggregation

Since different MCDA methods may produce different rankings, a rank aggregation step is introduced to obtain a more stable and consistent decision. Let $R^{(m)} = [r_{1m}, \ldots, r_{nm}]$ denote the ranking obtained from method m, where $m = 1, \ldots, M$.

For Borda count [11], each alternative is assigned a score based on its position in each ranking:

$$R_i^{\text{Borda}} = \frac{1}{M}\sum_{m=1}^{M}(n - r_{im}) \tag{21}$$

For Copeland index [30], pairwise comparisons are used. The number of wins and losses for each alternative i are computed as:

$$W_i = \sum_{j\neq i} I\left(r_i > r_j\right), L_i = \sum_{j\neq i} I\left(r_i < r_j\right) \Rightarrow \;\; C_i = W_i - L_i \tag{22}$$

For Kemeny–Young consensus [31], seeks a ranking R^* that maximizes agreement with all individual rankings:

$$R^* = \arg\max_R \sum_{m=1}^{M} \tau\left(R, R^{(m)}\right) \tag{23}$$

where τ is Kendall's tau between rankings.

For Robust Rank Aggregation (RRA) [32], each rank is first converted into a normalized value, $p_{im} = r_{im}/n$. The aggregated significance is then estimated by

$$P_i = \min_k \left(n \prod_{m=1}^{k} p_{im} \right)^{1/k}, \qquad \text{RRA}_i = -\log 10\,(P_i) \tag{24}$$

Consensus selection

The final consensus score integrates the results of the aggregation methods:

$$\overline{R_i} = \frac{R_i^{\text{Borda}} + C_i + R_i^{\text{Kemeny}} + \text{RRA}_i}{4} \tag{25}$$

The alternative with the highest $\overline{R_i}$ is selected as the recommended machining condition.

Experimental validation

Selected Pareto solutions (x^*) are experimentally verified on the same machine–tool–coolant configuration. The predicted and measured responses are compared using the absolute and relative errors:

$$E_j = \left|y_{j,\text{exp}} - y_{j,\text{pred}}\right|, \qquad RE_j(\%) = \frac{AE_j}{y_{j,\text{exp}}} \times 100 \tag{26}$$

Average relative error within 0-5 % for *Ra* and *MRR* indicates good agreement between predictions and experiment, supporting the reliability of the proposed workflow [24].

4. Results and discussion

4.1 Machine learning model performance

Table 2 reports the predictive accuracy of four surrogate models for *Ra* and *MRR*, using the same train/test split and preprocessing pipeline. Figs. 4 and 5 visualize the agreement between experimental and predicted values on the train and test partitions.

Table 2 Model performance metrics for *Ra* and *MRR*

Model	Surface roughness						Material removal rate					
	Train			Test			Train			Test		
	RMSE	MAE	R^2	RMSE	MAE	R^2	RMSE	MAE	R^2	RMSE	MAE	R^2
KAN	0.0082	0.006	0.999	0.0541	0.042	0.989	0.1343	0.100	0.999	0.5206	0.260	0.996
CAT	0.1012	0.078	0.983	0.0897	0.074	0.968	0.0040	0.003	0.999	2.2987	1.486	0.994
GBR	0.0017	0.001	0.999	0.0767	0.061	0.982	0.1180	0.072	0.999	4.6363	3.543	0.993
LGB	0.1920	0.138	0.941	0.0964	0.074	0.967	1.5290	1.090	0.989	4.7165	3.648	0.952

Surface roughness predictive performance

Across models, *Ra* is predicted with high fidelity, but the generalization gap differs markedly. KAN attains the best test performance (RMSE = 0.0541; MAE = 0.042; R^2 = 0.98), with only a slight drop from its near-perfect training fit (R^2 = 0.999). GBR ranks second on the test set (R^2 = 0.982; RMSE

= 0.0767), followed by CAT (R^2 = 0.968) and LGB (R^2 = 0.967). Notably, LGB shows the clearest sign of underfitting on *Ra* (train R^2 = 0.941; test RMSE = 0.192). Fig. 4 shows KAN lying closest to the 45° line, while tree-boosting models deviate more in the mid-high *Ra* range (1.5-2.5 μm).

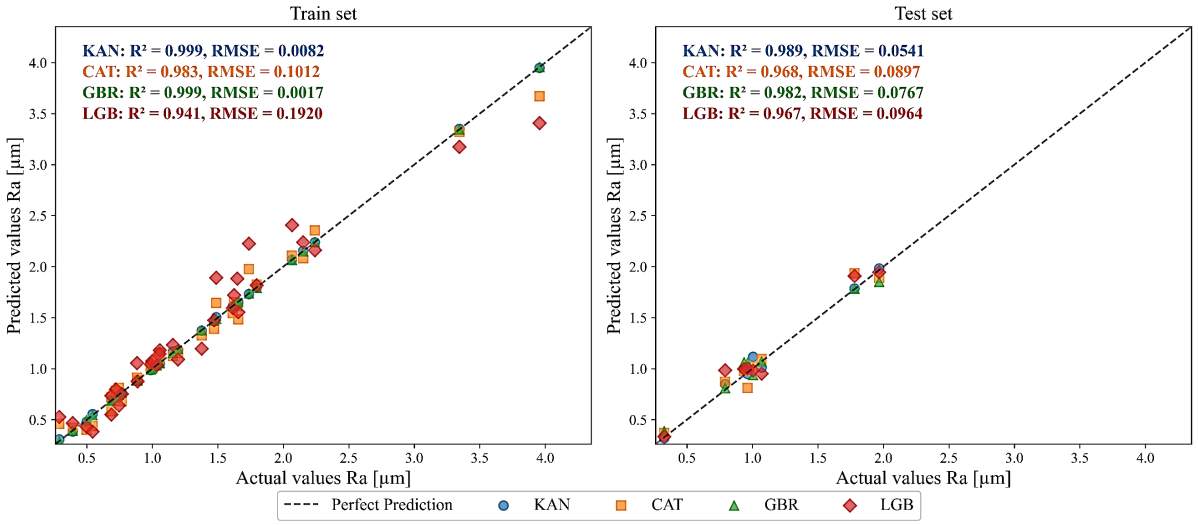

Fig. 4 Experimental vs. predicted values for Ra on train and test sets

Material removal rate predictive performance

Training fits are near-perfect for all, but their out-of-sample behavior diverges. KAN again provides the strongest generalization (test RMSE = 0.5206; R^2 = 0.999), keeping errors at a sub-percent scale relative to the *MRR* range in Fig. 5. In contrast, CAT degrades to RMSE = 2.2987 (R^2 = 0.994); meanwhile, GBR and LGB show larger errors (RMSE = 4.6363 and 4.7165; R^2 = 0.993 and 0.952). Fig. 5 indicates systematic under-prediction at high *MRR* for tree-based models, whereas KAN preserves the trend with minimal bias. Based on the test-set results, KAN showed the strongest generalization for both *Ra* and *MRR* and was therefore retained as the surrogate model for both responses in the subsequent optimization stage.

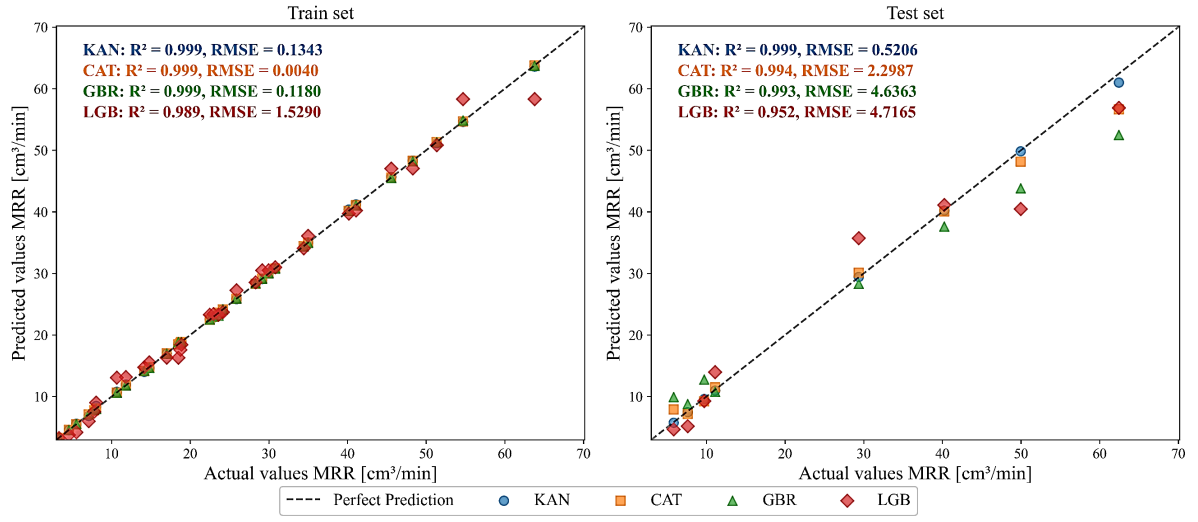

Fig. 5 Experimental vs. predicted values for *MRR* on train and test sets

4.2 Machine learning model explanation

Model explanation for Ra

Fig. 6a highlights the darkest branches from *f* and nose radius R_E, with weaker links from *ap*, *Vc*, and *CL*; this ordering is confirmed by the KAN feature scores in Fig. 6b and the GBR-SHAP violins in Fig. 6c, where high *f* shifts *Ra* upward while large R_E shifts it downward. The dominance of feed

on roughness for brass is consistent with recent turning studies on Ms58, CW614N and other copper alloys, which report a substantial, monotonic increase of *Ra* with rising feed due to a thicker undeformed chip and more pronounced feed marks [33]. In parallel, the nose radius acts as a geometric smoother: larger R_E lowers cusp height and improves finish in brass andcopper alloys, a trend echoed by brass-focused machinability reports and broader turning investigations on nose-radius effects [34]. Regarding cutting speed, *Ra* tends to decrease as V_c increases because higher speed suppresses adhesion and built-up edge in lead-free brasses, improving surface topography—again matching the slight negative SHAP trend for V_c [35]. The influence of depth of cut on *Ra* is secondary within our range, mainly through force and vibration pathways; copper-alloy turning with coated tools similarly finds feed most influential and depth-of-cut a weaker contributor to roughness [36]. Finally, coolant shows only a minor direct effect on *Ra* for brass in our DOE, although tailored lubrication or hybrid cryo-MQL can still yield incremental finish improvements—consistent with brass turning tests and recent lead-free brass studies [37].

$$\begin{aligned} Ra = {} & 0.19\,x_1 - 0.06\,x_3 - 0.34\,x_4 + 0.03\,x_5 + 0.02\,e^{0.94\,x_1} \\ & +0.16\,e^{1.24\,x_1} - 0.02e^{0.69\,x_2} - 0\cdot 10^{-2}e^{0.72\,x_2} + 0.01\,e^{1.06\,x_3} + 1.8 \\ & +0.01\,e^{-0.86\,x_1} - 0.11\,e^{-0.12\,x_1} \end{aligned} \tag{27}$$

With $[x_1, x_2, x_3, x_4, x_5] = [f, V_c, a_p, R_E, CL]$, *Ra* is driven mainly by feed: positive linear and exponential terms in x_1 make *Ra* increase with *f*. Speed enters only via negative exponentials in x_2, so higher V_c lowers *Ra* with a saturating effect. Depth of cut has a weak net influence (small positive exponential offset by a negative linear term). The negative linear term in x_4 shows a larger R_E smooths the surface. The *CL* term is tiny, indicating a negligible direct effect in this DOE.

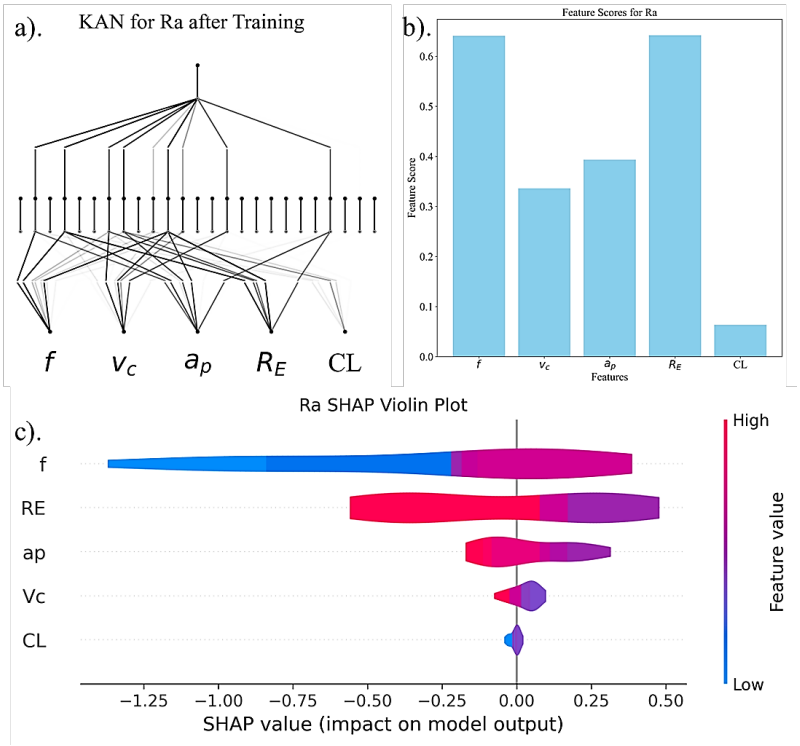

Fig. 6 Explanation for *Ra*: (a) KAN for initialization, (b) KAN feature importance, (c) GBR SHAP violin

Model explanation for MRR

Fig. 7a shows the branches from a_p, V_c, and f to *MRR* with high, medium, and lower intensity, respectively, while the links from R_E and *CL* are very faint—indicating negligible direct influence. This is reinforced in Fig. 7b, the feature-importance plot ranks ap highest, followed by V_c and f, with R_E and *CL* close to zero. Fig. 7c indicates the direction of effects: SHAP distributions for ap and V_c lie mainly on the positive side, and the pink (high-value) portions on the right show that

larger a_p or V_c increase *MRR*; the blue segments on the left indicate that smaller values reduce *MRR*. For *f*, the trend is similar but with a smaller magnitude; R_E and *CL* concentrate around zero.

$$MRR = 0.26\,x_3 + 0.28\,e^{0.34\,x_2} + 0.66\,e^{0.48\,x_3+0.91\,e^{0.25\,x_2}-0.37\,e^{-0.55\,x_1}} \\ -1.44 - 0\cdot 10^{-2}e^{-0.6\,x_5} - 0.14\,e^{-0.61\,x_1} \tag{28}$$

The positive linear term $0.26x_3$ and the exponential term containing x_3 confirm the dominant role of a_p; positive exponentials in x_2 capture the increase of *MRR* with V_c; the $-0.14\,e^{-0.61\,x_1}$ term explains a amplified contribution from *f* within the tested range; the *CL* coefficient is effectively zero and R_E does not appear—consistent with Fig. 7.

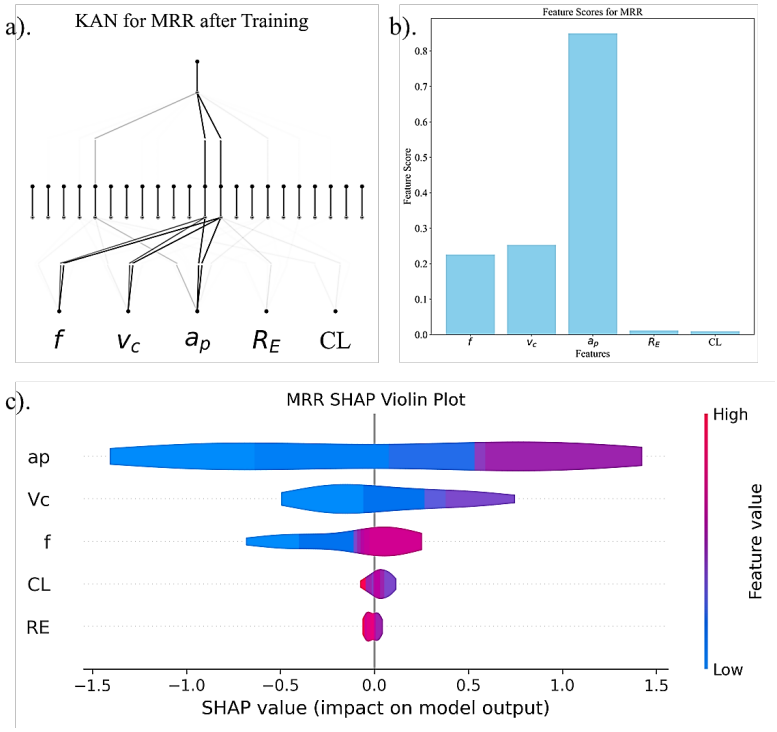

Fig. 7 Explanation for *MRR*: (a) KAN for initialization, (b) KAN feature importance, (c) CAT-SHAP violin

4.3 NSGA-III Multi-Objective optimization

Having established reliable surrogates, we used NSGA-III to identify Pareto-optimal settings that minimize *Ra* and maximize *MRR*. The algorithm ran with a population of 50 for 50 generations, using simulated binary crossover and polynomial mutation to maintain diversity. Similar evolutionary strategies have proved effective for complex manufacturing optimization [10].

Fig. 8a shows the final Pareto front from NSGA-III (*Ra* in range of 0.45-1.644 μm; *MRR* in range of 29.724-80.62 cm^3/min), while Fig. 8b, the hypervolume increases rapidly and then stabilizes, indicating convergence. Fig. 9 overlays the frontier on the DOE trials, confirming the expected trade-off—lower *Ra* comes at the cost of lower *MRR*—and the advantage of model-based search over trial-and-error [38]. In terms of operating windows, our "finish-first" range (*Ra* about 0.45-1.0 μm at low feed and higher speed) agrees with recent brass-turning studies reporting that reducing feed and increasing cutting speed improve surface finish; the "productivity-first" range (*Ra* about 1.3-1.6 μm with *MRR* 70-81 cm^3/min) corresponds to higher feed and depth, consistent with the literature on kinematic drivers of *MRR* [37]. Although a smaller R_E can minimize *Ra* when the feed is kept low (Fig. 6), the multi-objective context favors R_E = 0.8 mm in 8 of the 9 Pareto solutions (Table 3) because a larger nose radius acts as a geometric smoother that permits higher feed at comparable *Ra*, thereby lifting *MRR* without breaching the finish target [33].

Table 3 Optimal solutions generated by NSGA-III

Solution	f (mm/rev)	V_c (m/min)	a_p (mm)	R_E (mm)	CL	Ra (μm)	MRR (cm³/min)
1	0.114	176.948	1.501	1	0	0.450	29.724
2	0.121	224.867	1.475	1	0	0.585	39.990
3	0.122	221.061	1.842	0	0	0.704	48.373
4	0.133	224.893	1.848	1	0	0.810	55.030
5	0.146	224.893	1.850	1	0	0.945	59.575
6	0.160	224.824	1.849	1	0	1.104	64.060
7	0.185	224.996	1.764	1	0	1.222	69.437
8	0.194	224.970	1.837	1	0	1.322	75.249
9	0.210	224.981	1.850	1	0	1.644	80.620

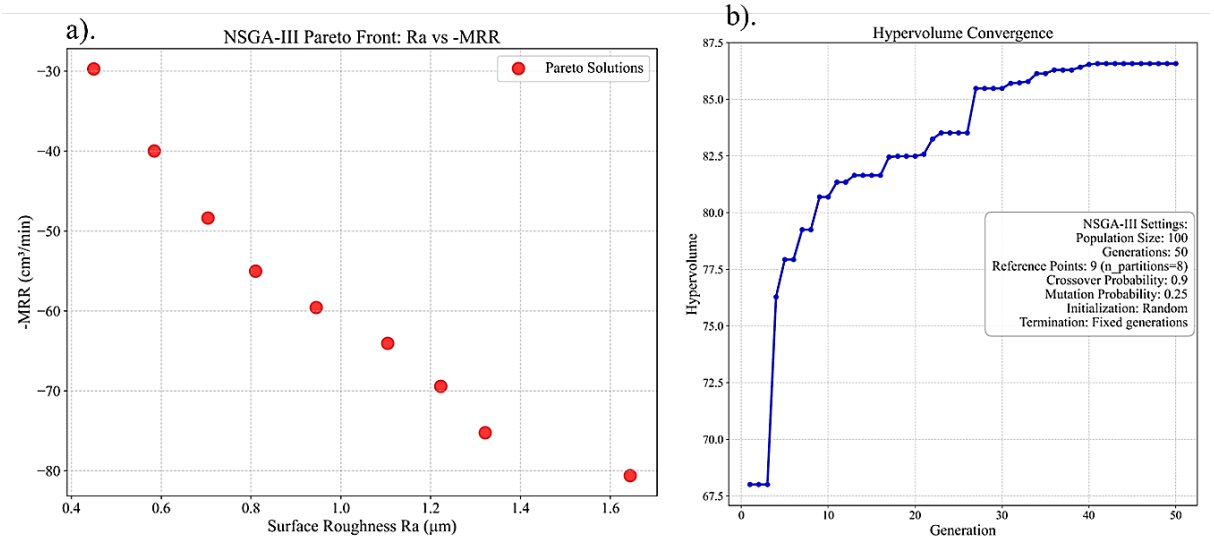

Fig 8 NSGA-III results: (a) Pareto front in the *Ra*-(−*MRR*) space. (b) Hypervolume convergence across generations

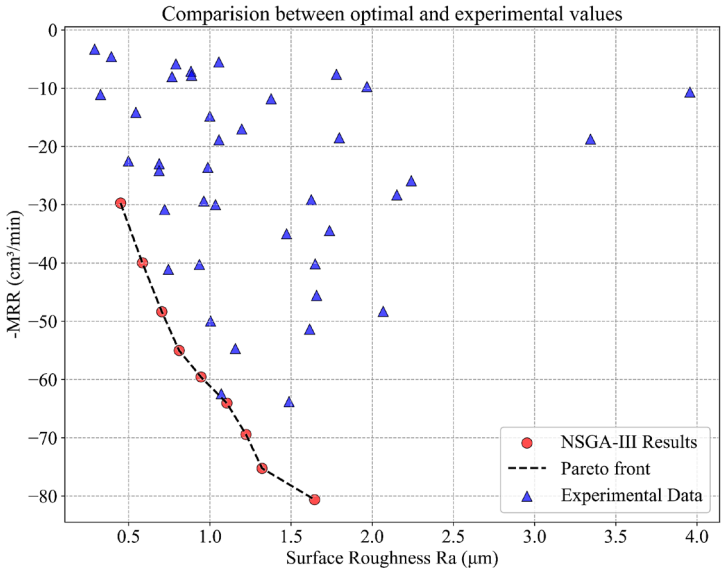

Fig. 9 Comparison of NSGA-III Pareto-optimal solutions with experimental trials in the *Ra* and (−*MRR*) space

4.4 MCDM-Based selection of the best solution

Although the Pareto front provides multiple feasible choices, industrial decision-makers often need a single recommended solution. This study applied four MCDM methods—CODAS, SPOTIS, MABAC, and WASPAS—to the Pareto-optimal set. The various weighting methods objectively assigned weights to the criteria, eliminating subjective biases.

Table 4 summarizes the Entropy, Gini, and MEREC weights for *Ra* and *MRR*. Table 5 reports, for each weighting scheme, the preference scores and induced ranks across the four MCDA methods; Fig. 10 visualizes the resulting orderings. Under Entropy weighting, all four methods rank Solution 1 first. Under Gini, most methods still favor Solution 1, with MABAC ranking Solution 4 first. Under MEREC, CODAS, SPOTIS, and WASPAS again select Solution 1, whereas MABAC prefers Solution 8. These modest disagreements across methods are typical in MCDA and motivate a principled consensus step.

To reduce weighting method sensitivity, four aggregators—Borda, Copeland, Kemeny–Young, and Robust Rank Aggregation—were applied to the per-method ranks (Table 6; Fig. 11). All four aggregators concur on Solution 1 as the overall best candidate, with Solutions 2-3 following and Solution 9 consistently last. The cross-method agreement indicates that the selected operating point is robust to reasonable changes in weighting and MCDA formulation, in line with recommendations to use consensus procedures when multiple ranking rules are plausible.

Table 4 Calculation weights for various objectives

Objective	MEREC	Entropy	Gini	Type
Ra	0.481	0.642	0.578	cost
MRR	0.519	0.358	0.422	benefit

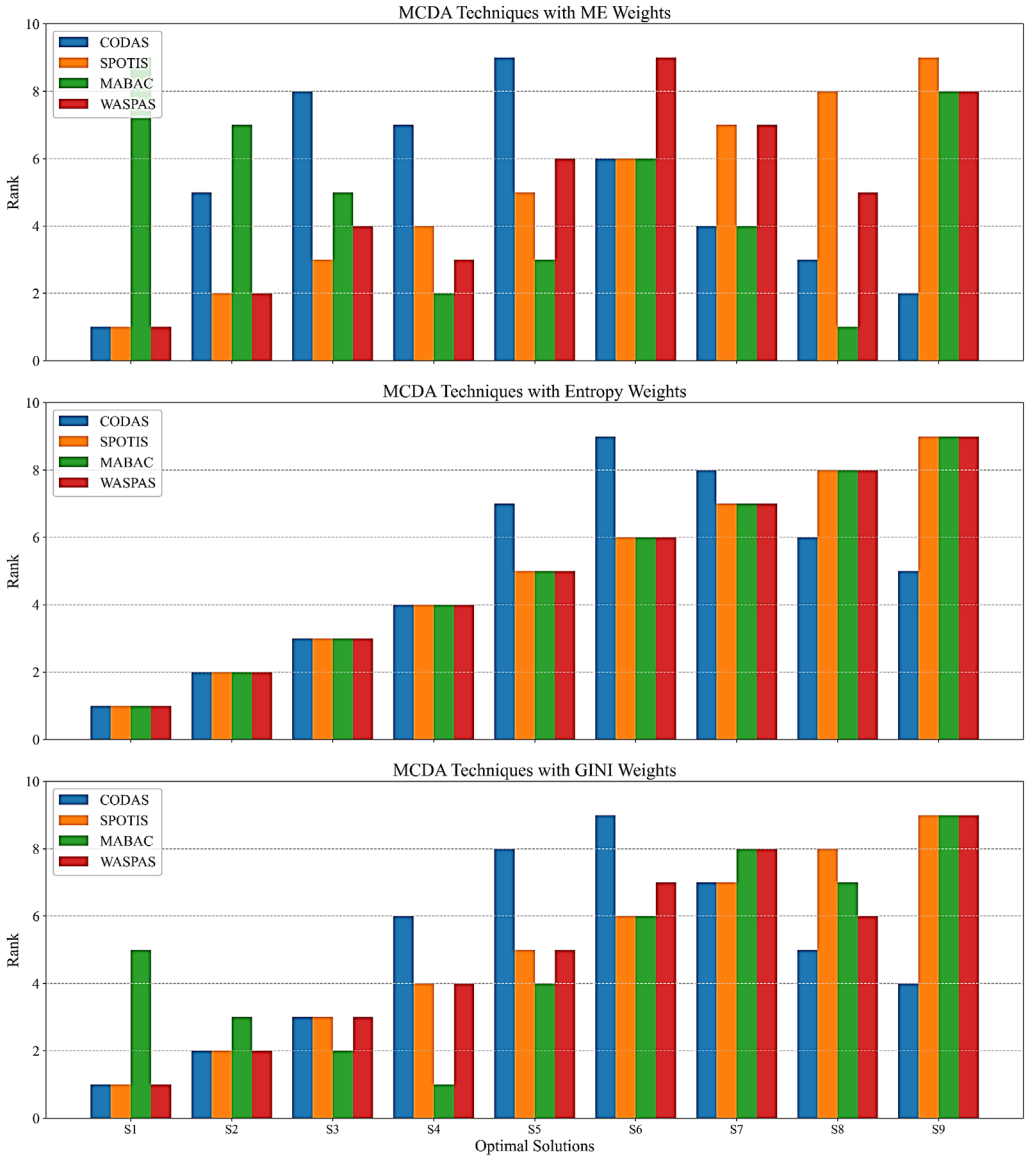

Fig. 10 Ranking of selected solutions by various MCDM methods with various weights

Table 5 MCDM-based ranking of selected Pareto solutions

ENTROPY	CODAS	pref	3.52	1.30	0.22	-0.44	-0.90	-1.14	-1.04	-0.79	-0.73
		rank	1	2	3	4	7	9	8	6	5
	SPOTIS	pref	0.23	0.19	0.15	0.12	0.11	0.09	0.07	0.04	0.03
		rank	1	2	3	4	5	6	7	8	9
	MABAC	pref	0.12	0.12	0.11	0.10	0.06	0.01	-0.02	-0.03	-0.17
		rank	1	2	3	4	5	6	7	8	9
	WASPAS	pref	0.74	0.66	0.62	0.60	0.56	0.53	0.52	0.52	0.48
		rank	1	2	3	4	5	6	7	8	9
GINI	CODAS	pref	2.59	0.72	-0.17	-0.51	-0.76	-0.83	-0.59	-0.27	-0.18
		rank	1	2	3	6	8	9	7	5	4
	SPOTIS	pref	0.27	0.22	0.18	0.14	0.12	0.10	0.07	0.05	0.02
		rank	1	2	3	4	5	6	7	8	9
	MABAC	pref	0.05	0.07	0.08	0.09	0.06	0.02	0.01	0.01	-0.10
		rank	5	3	2	1	4	6	8	7	9
	WASPAS	pref	0.70	0.65	0.62	0.61	0.58	0.56	0.55	0.56	0.53
		rank	1	2	3	4	5	7	8	6	9
MEREC	CODAS	pref	1.17	-0.18	-0.56	-0.56	-0.57	-0.44	-0.08	0.45	0.77
		rank	1	5	8	7	9	6	4	3	2
	SPOTIS	pref	0.33	0.27	0.22	0.17	0.15	0.12	0.09	0.05	0.02
		rank	1	2	3	4	5	6	7	8	9
	MABAC	pref	-0.04	0.01	0.04	0.07	0.06	0.04	0.05	0.07	-0.01
		rank	9	7	5	2	3	6	4	1	8
	WASPAS	pref	0.63	0.62	0.62	0.62	0.61	0.59	0.60	0.61	0.59
		rank	1	2	4	3	6	9	7	5	8

Table 6 Rank aggregation of Pareto solutions: Borda, Copeland, Kemeny–Young, RRA, and final consensus rank

Solution	Borda	Copeland	KemenyYoung	RRA	Final rank
1	1	1	1	1	1
2	2	2	2	2	2
3	3	3	3	3	3
4	4	4	4	4	4
5	5	5	5	7	5
6	8	6	6	8	8
7	7	8	8	5	7
8	6	7	7	6	6
9	9	9	9	9	9

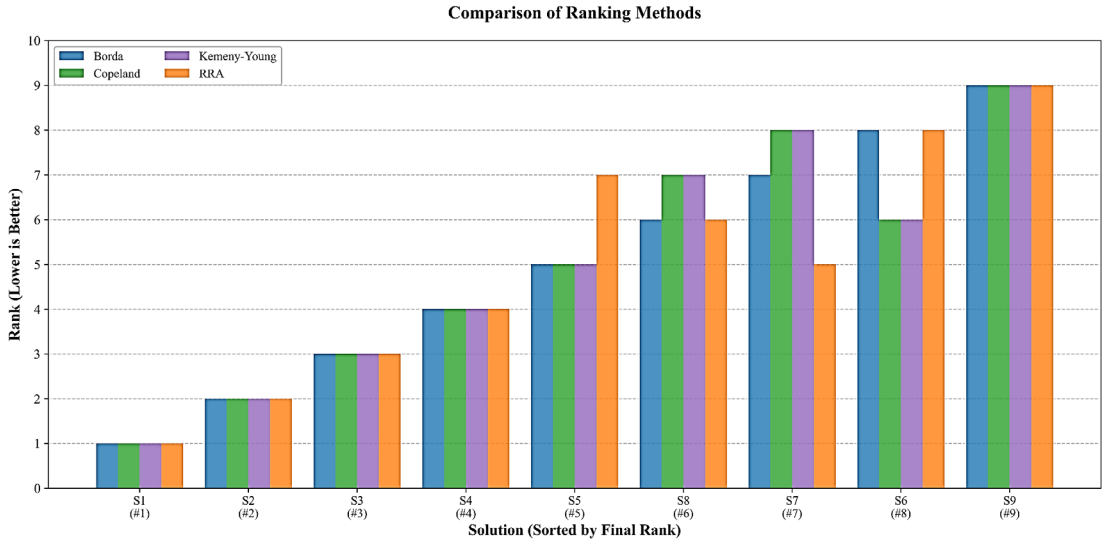

Fig. 11 Comparison of rank-aggregation methods for Pareto candidates—Borda, Copeland, Kemeny–Young, and RRA (solutions ordered by final consensus rank)

Taken together, the evidence from Tables 4-6 and Fig. 10 indicate that Solution 1 is the most suitable choice and is selected for experimental confirmation.

4.5 Experimental confirmation

Validation cuts were conducted at the consensus point S1 and two neighboring points (S2 and S3) using the same machine, fixturing, and coolant condition. Each setting was repeated three times (n = 3) with a fresh cutting edge. *Ra* and *MRR* were identified in the Section 3 procedure. Accuracy was assessed using AE_j and RE_j(%) as defined in Eq. 26. The predefined acceptance criterion was $RE_j(\%) \leq 5$ % for both *Ra* and *MRR*. Results in Table 7 indicate close agreement between predictions and measurements; the pattern across S_1–S_3 also confirms the *Ra*–*MRR* trade-off observed on the Pareto front. In practice, the confirmation supports R_E = 0.8 mm as the joint optimum: although a smaller R_E can minimize *Ra* in isolation, the larger radius permits higher *f* at comparable *Ra*, thereby increasing *MRR* without breaching finish targets.

This work presents an integrated data-to-decision workflow for machining optimization, combining surrogate modeling, explainability, multi-objective optimization, and MCDA within a single procedure. Rather than relying on a single model or a fixed decision rule, the approach evaluates the trade-off between surface quality and productivity under multiple weighting and ranking settings, leading to a more consistent basis for selecting the final operating condition.

An important aspect of this study is that the final decision is not tied to a single weighting scheme or ranking method. Instead, several weighting approaches and MCDA methods are considered, and their results are combined through rank aggregation [35]. This reduces the dependence on any individual method and helps obtain a more stable and technically balanced recommendation. The experimental validation further shows that the selected solutions remain close to the predicted values, supporting the practical applicability of the proposed workflow. At the same time, the present validation should be interpreted within the scope of the selected objectives. In this study, *Ra* and *MRR* were used as representative quality and productivity responses to demonstrate the workflow in a focused turning case study. In broader industrial applications, however, the final operating condition may also need to account for factors such as tool life, cutting-force stability, machining efficiency, and processing time.

Table 7 Experimental confirmation at Pareto points (mean ± SD over n = 3)

Setting	Cutting conditions	Ra_{pred}	Ra_{exp}	AE (μm)	RE (%)	MRR_{pred}	MRR_{exp}	AE (cm^3/min)	RE (%)
S1	f = 0.114, V_c = 176.948, a_p = 1.50, R_E = 0.8, CL = 0	0.450	0.468 ± 0.012	0.018	3.85	29.724	29.48 ± 0.30	0.244	0.83
S2	f = 0.121, V_c = 224.867, a_p = 1.475, R_E = 0.8, CL = 0	0.585	0.602 ± 0.015	0.017	2.82	39.990	39.35 ± 0.45	0.640	1.63
S3	f = 0.122, V_c = 221.061, a_p = 1.842, R_E = 0.4, CL = 0	0.704	0.741 ± 0.019	0.037	4.99	48.373	47.55 ± 0.55	0.823	1.73

5. Conclusion

This study presents a complete data-to-decision workflow for machining optimization with limited data. The workflow combines surrogate modeling with Bayesian tuning, NSGA-III for generating the *Ra*–*MRR* Pareto front, and a decision layer based on MCDA with objective weighting and rank aggregation. For the C3604 brass case, this procedure led to a single final operating condition and was further checked by experiment.

The main findings are as follows:

- The surrogate comparison among KAN, CAT, GBR, and LGB under a unified pipeline showed good generalization on held-out data.
- NSGA-III generated a well-distributed Pareto front, and the hypervolume results indicated stable search behavior.
- The MCDA methods (CODAS, SPOTIS, MABAC, and WASPAS) combined with Entropy, Gini, and MEREC weights produced only minor differences in ranking.
- Rank aggregation using Borda, Copeland, Kemeny–Young, and RRA gave a stable consensus, with Solution 1 ranked first overall.
- Experimental tests at representative Pareto points agreed well with the predictions, with relative errors below 5 % for both *Ra* and *MRR*.

This study considered only two responses, *Ra* and *MRR*, and did not include energy, force constraints, or tool wear in the optimization stage. In addition, predictive uncertainty and robust optimization were not treated explicitly. Although the proposed data-to-decision framework is general in structure and can be adapted to other machining systems with different machine configurations, input variables, and output responses, the numerical recommendation obtained in the present C3604 turning case study remains specific to the investigated experimental domain and should not be directly transferred to other machines, tool systems, or coolant settings without re-evaluation.

Future work will extend the framework to include additional objectives such as energy and cost, incorporate wear-related responses, and develop uncertainty-aware decision strategies. A lightweight calibration step across different machines and a real-time GUI for shop-floor use are also planned.

References

[1] Abdelaoui, F.Z.E., Jabri, A., Barkany, A.E. (2023). Optimization techniques for energy efficiency in machining processes-a review, *The International Journal of Advanced Manufacturing Technology*, Vol. 125, No. 7-8, 2967-3001, doi: 10.1007/s00170-023-10927-y.

[2] Tang, K.-E., Lin, G.-Y., Liu, C.-W. (2025). Sustainable orthogonal turn-mill process parameter decision-making based on specific consumption energy model and NSGA-II multi-objective optimization algorithm, *The International Journal of Advanced Manufacturing Technology*, Vol. 137, No. 11-12, 6107-6121, doi: 10.1007/s00170-025-15490-2.

[3] Nguyen, V.-H., Le, T.-T., Le, M.V., Dao Minh, H., Nguyen, A.-T. (2023). Multi-objective optimization based on machine learning and non-dominated sorting genetic algorithm for surface roughness and tool wear in Ti_6Al_4V turning, *Machining Science and Technology*, Vol. 27, No. 4, 380-421, doi: 10.1080/10910344.2023.2235610.

[4] Al-Samarai, R.A., Al-Douri, Y. (2025). *Advanced cutting tool technology and machine processes*, CRC Press, Boca Raton, Florida, USA, doi: 10.1201/9781003604648.

[5] Nguyen, V.-H., Le, T.-T., Nguyen, A.-T., Hoang, X.-T., Nguyen, N.-T., Nguyen, N.-K. (2025). Optimization of milling conditions for AISI 4140 steel using an integrated machine learning-multi objective optimization-multi criteria decision making framework, *Measurement*, Vol. 242, Part A, Article No. 115837, doi: 10.1016/j.measurement.2024.115837.

[6] Zhou, A., Zhang, Q., Zhang, G. (2012). A multiobjective evolutionary algorithm based on decomposition and probability model, In: *Proceedings of 2012 IEEE Congress on Evolutionary Computation (CEC)*, Brisbane, Australia, 1-8, doi: 10.1109/CEC.2012.6252954.

[7] Vu, B.D., Tran, G.N., Dinh, V.T., Bui, H.T., Do, T.T. (2026). Minimizing the cross-sectional area and maximizing efficiency in split-input two-stage gearboxes via NSGA-II with SAW-guided choice, *Engineering, Technology & Applied Science Research*, Vol. 16, No. 1, 31916-31922, doi: 10.48084/etasr.14925.

[8] Nguyen, V.-H., Le, T.-T., Nguyen, A.-T., Hoang, X.-T., Nguyen, N.-T. (2025). Comprehensive machine learning and multi-criteria optimization workflow for trochoidal milling parameter selection in AISI 4140 steel, *The International Journal of Advanced Manufacturing Technology*, Vol. 141, 4071-4094, doi: 10.1007/s00170-025-16916-7.

[9] Sofianidis, G., Rožanec, J.M., Mladenić, D., Kyriazis, D. (2021). A review of explainable artificial intelligence in manufacturing, In: Soldatos, J., Kyriazis, D. (eds.), *Trusted artificial intelligence in manufacturing: A review of the emerging wave of ethical and human centric AI technologies for smart production*, Emerald Publishing Limited, Leeds, United Kingdom, 93-113, doi: 10.1561/9781680838770.ch5.

[10] Deb, K., Pratap, A., Agarwal, S., Meyarivan, T. (2002). A fast and elitist multiobjective genetic algorithm: NSGA-II, *IEEE Transactions on Evolutionary Computation*, Vol. 6, No. 2, 182-197, doi: 10.1109/4235.996017.

[11] Liu, Q., Jing, Y., Yan, Y., Li, Y. (2024). Mean-based Borda count for paradox-free comparisons of optimization algorithms, *Information Sciences*, Vol. 660, Article No. 120120, doi: 10.1016/j.ins.2024.120120.

[12] Keshavarz-Ghorabaee, M., Amiri, M., Zavadskas, E.K., Turskis, Z., Antucheviciene, J. (2021). Determination of objective weights using a new method based on the removal effects of criteria (MEREC), *Symmetry*, Vol. 13, No. 4, Article No. 525, doi: 10.3390/sym13040525.

[13] Vukelic, D., Milosevic, A., Ivanov, V., Kocovic, V., Santosi, Z., Sokac, M., Simunovic, G. (2024). Modelling and optimization of dimensional accuracy and surface roughness in dry turning of Inconel 625 alloy, *Advances in Production Engineering & Management*, Vol. 19, No. 3, 371-385, doi: 10.14743/apem2024.3.513.

[14] Milosevic, A., Simunovic, G., Kanovic, Z., Simunovic, K., Kocovic, V., Vukelic, D. (2025). Modelling and optimization of surface quality and productivity in turning Inconel 825 alloy, *International Journal of Simulation Modelling*, Vol. 24, No. 4, 565-576, doi: 10.2507/IJSIMM24-4-725.

[15] While, L., Hingston, P., Barone, L., Huband, S. (2006). A faster algorithm for calculating hypervolume, *IEEE Transactions on Evolutionary Computation*, Vol. 10, No. 1, 29-38, doi: 10.1109/TEVC.2005.860074.

[16] Ullah, A., Chan, T.-C., Chang, S.-L. (2025). Current trends in vibration control and computational optimization for CNC machine tools: A comprehensive review, *The International Journal of Advanced Manufacturing Technology*, Vol. 139, 5409-5444, doi: 10.1007/s00170-025-16238-8.

[17] Bartels, S., Boomsma, W., González-Duque, M., Hauberg, S., Michael, R., Zainchkovskyy, Y. (2024). A survey and benchmark of high-dimensional Bayesian optimization of discrete sequences, In*: Proceedings of Advances in Neural Information Processing Systems 37,* Vancouver, Canada, 140478-140508, doi: 10.52202/079017-4459.
[18] Wang, H., Bai, Q., Chen, S., Wang, T., Guo, W., Dou, Y. (2025). Neural networks with dual-view fusion feature learning mechanism: A method to improve micro-milling tool wear monitoring performance by enhancing feature generalization capabilities, *Mechanical Systems and Signal Processing*, Vol. 236, Article No. 113038, doi: 10.1016/j.ymssp.2025.113038.
[19] Lundberg, S.M., Lee, S.-I. (2017). A unified approach to interpreting model predictions, In: *Proceedings of 31st Conference on Neural Information Processing Systems (NIPS 2017),* Long Beach, USA, 4768-4777.
[20] Liu, Z., Wang, Y., Vaidya, S., Ruehle, F., Halverson, J., Soljačić, M., Hou, T.Y., Tegmark, M. (2024). KAN: Kolmogorov-Arnold networks, *arXiv*, doi: 10.48550/arXiv.2404.19756.
[21] Deb, K., Jain, H. (2014). An evolutionary many-objective optimization algorithm using reference-point-based nondominated sorting approach, part I: Solving problems with box constraints, *IEEE Transactions on Evolutionary Computation*, Vol. 18, No. 4, 577-601, doi: 10.1109/TEVC.2013.2281535.
[22] Zavadskas, E.K., Antuchevičienė, J., Šaparauskas, J., Turskis, Z. (2013). MCDM methods WASPAS and MULTIMOORA: Verification of robustness of methods when assessing alternative solutions, *Economic Computation and Economic Cybernetics Studies and Research*, Vol. 47, No. 2, 5-20.
[23] Pamučar, D., Ćirović, G. (2015). The selection of transport and handling resources in logistics centers using Multi-Attributive Border Approximation area Comparison (MABAC), *Expert Systems with Applications*, Vol. 42, No. 6, 3016-3028, doi: 10.1016/j.eswa.2014.11.057.
[24] Montgomery, D.C. (2017). *Design and analysis of experiments*, 9th edition, John Wiley & Sons, Hoboken, New Jersey, USA.
[25] Nguyen, V.-H., Le, T.-T., Truong, H.-S., Le, M.V., Ngo, V.-L., Nguyen, A.T., Nguyen, H.Q. (2021). Applying Bayesian optimization for machine learning models in predicting the surface roughness in single-point diamond turning polycarbonate, *Mathematical Problems in Engineering*, Vol. 2021, No. 1, Article No. 6815802, doi: 10.1155/2021/6815802.
[26] Snoek, J., Larochelle, H., Adams, R.P. (2012). Practical Bayesian optimization of machine learning algorithms, In: *Proceedings of Advances in Neural Information Processing Systems 25 (NIPS 2012),* Lake Tahoe, Nevada, USA, 2951-2959.
[27] Li, G., Chi, G. (2009). A new determining objective weights method-Gini coefficient weight, In: *Proceedings of 2009 First International Conference on Information Science and Engineering*, Nanjing, China, 3726-3729, doi: 10.1109/ICISE.2009.84.
[28] Keshavarz Ghorabaee, M., Zavadskas, E.K., Turskis, Z., Antucheviciene, J. (2016). A new combinative distance-based assessment (CODAS) method for multi-criteria decision-making, *Economic Computation and Economic Cybernetics Studies and Research*, Vol. 50, No. 3, 25-44.
[29] Shekhovtsov, A., Dezert, J., Sałabun, W. (2024). Generalization of stable preference ordering towards ideal solution approach for working with imprecise data, *Operations Research and Decisions*, Vol. 34, No. 3, 243-266, doi: 10.37190/ord2403013.
[30] Özdağoğlu, A., Keleş, M.K., Altınata, A., Ulutaş, A. (2021). Combining different MCDM methods with the Copeland method: An investigation on motorcycle selection, *Journal of Process Management and New Technologies*, Vol. 9, No. 3-4, 13-27, doi: 10.5937/jouproman2103013O.
[31] Phung, X.K., Hamel, S. (2025). Efficient space reduction techniques by optimized majority rules for the Kemeny aggregation problem and beyond, *arXiv*, doi: 10.48550/arXiv.2506.15097.
[32] Võsa, U., Kolde, R., Vilo, J., Metspalu, A., Annilo, T. (2014). Comprehensive meta-analysis of MicroRNA expression using a robust rank aggregation approach, In: Alvarez, M.L., Nourbakhsh, M. (eds.), *RNA Mapping. Methods in Molecular Biology,* Vol. 1182, Humana Press, New York, USA, 361-373, doi: 10.1007/978-1-4939-1062-5_28.
[33] Ateş, E., Serbest, N. (2024). Investigation of effects of feed rate and cutting-edge angle variation on surface roughness in external cylindrical turning process of Ms58 brass material, *Applied Sciences*, Vol. 14, No. 24, Article No. 12039, doi: 10.3390/app142412039.
[34] Atay, G., Zoghipour, N., Kaynak, Y. (2023). Investigation of machining performance of lead-free brass materials forged in different conditions after cooling with liquid nitrogen, In*: Proceedings of The 26th International Esaform Conference on Material Forming, ESAFORM 2023,* Krakow, Poland, Vol. 28, 1357-1366, doi: 10.21741/9781644902479-147.
[35] Das, A., Bajpai, V. (2023). Machinability analysis of lead free brass in high speed micro turning using minimum quantity lubrication, *CIRP Journal of Manufacturing Science and Technology*, Vol. 41, 180-195, doi: 10.1016/j.cirpj.2022.11.023.
[36] Mohanta, D.K., Sahoo, B., Mohanty, A.M. (2024). Experimental analysis for optimization of process parameters in machining using coated tools, *Journal of Engineering and Applied Science*, Vol. 71, Article No. 38, doi: 10.1186/s44147-024-00370-5.
[37] Hussein, S.G. (2014). An experimental study of the effects of coolant fluid on surface roughness in turning operation for brass alloy, *Journal of Engineering*, Vol. 20, No. 3, 96-104, doi: 10.31026/j.eng.2014.03.09.
[38] Shrivastava, A., Pandey, M. (2024). Integrating and optimizing quality and client satisfaction in resource constrained time-cost trade-off for construction projects with NSGA-III methodology, *Asian Journal of Civil Engineering*, Vol. 25, 5669-5684, doi: 10.1007/s42107-024-01137-2.